El Niño drought increased canopy turnover in Amazon forests

Veronika Leitold[1,2], Douglas C. Morton[1] (iD), Marcos Longo[3] (iD), Maiza Nara dos-Santos[3], Michael Keller[3,4,5] and Marcos Scaranello[3]

[1]NASA Goddard Space Flight Center, Greenbelt, MD 20771, USA; [2]Department of Geographical Sciences, University of Maryland, College Park, MD 20742, USA; [3]EMBRAPA Informática Agropecuária, Barão Geraldo, Campinas, 13083-886, SP, Brazil; [4]NASA Jet Propulsion Laboratory, Pasadena, CA 91109, USA; [5]USDA Forest Service, International Institute of Tropical Forestry, Rio Piedras, PR 00926, USA

Author for correspondence:
Douglas C. Morton
Tel: +1 301 614 6688
Email: douglas.morton@nasa.gov

Summary

• Amazon droughts, including the 2015–2016 El Niño, may reduce forest net primary productivity and increase canopy tree mortality, thereby altering both the short- and the long-term net forest carbon balance. Given the broad extent of drought impacts, inventory plots or eddy flux towers may not capture regional variability in forest response to drought.

• We used multi-temporal airborne Lidar data and field measurements of coarse woody debris to estimate patterns of canopy turnover and associated carbon losses in intact and fragmented forests in the central Brazilian Amazon between 2013–2014 and 2014–2016.

• Average annualized canopy turnover rates increased by 65% during the drought period in both intact and fragmented forests. The average size and height of turnover events was similar for both time intervals, in contrast to expectations that the 2015–2016 El Niño drought would disproportionally affect large trees. Lidar–biomass relationships between canopy turnover and field measurements of coarse woody debris were modest ($R^2 \approx 0.3$), given similar coarse woody debris production and Lidar-derived changes in canopy volume from single tree and multiple branch fall events.

• Our findings suggest that El Niño conditions accelerated canopy turnover in central Amazon forests, increasing coarse woody debris production by 62% to $1.22\,\mathrm{Mg\ C\ ha^{-1}\ yr^{-1}}$ in drought years .

Introduction

Tropical rainforests play an important role in the global carbon cycle by sequestering atmospheric CO_2 in woody biomass (Le Quéré *et al.*, 2016). The Amazon is the largest remaining intact tropical forest in the world, and Amazon forests therefore have a strong influence on the magnitude and interannual variability in the global terrestrial carbon sink (Gatti *et al.*, 2014; Brienen *et al.*, 2015). The net carbon balance of the Amazon also reflects emissions from growing human pressure in the form of deforestation, degradation and fragmentation (Aguiar *et al.*, 2012; Longo *et al.*, 2016; Brinck *et al.*, 2017; van der Werf *et al.*, 2017). In recent years, natural disturbances associated with severe droughts and widespread forest fires initiated by humans have turned the Amazon from a net carbon sink into a net carbon source (Phillips *et al.*, 2009; Lewis *et al.*, 2011; Gatti *et al.*, 2014; Feldpausch *et al.*, 2016). However, large uncertainties remain regarding the magnitude of carbon fluxes in tropical forests (Pan *et al.*, 2011) and the underlying spatial distribution of carbon stocks across the landscape (e.g. Avitabile *et al.*, 2016; Longo *et al.*, 2016).

An improved understanding of the processes of forest disturbance and recovery is critical to constrain estimates of current and future carbon cycling in Amazon forests, including the size

and frequency of turnover events (Lloyd *et al.*, 2009). Forest inventory plots can estimate tree mortality with great precision (Phillips *et al.*, 2009; Brienen *et al.*, 2015; Feldpausch *et al.*, 2016), but plots sample a very small proportion of the Amazon and may not capture landscape-scale processes. At the other extreme, satellite observations can monitor large forested regions (Chambers *et al.*, 2013; Hansen *et al.*, 2013), but moderate resolution (30 m) data retain little sensitivity to small-scale changes in the forest canopy from branch and tree fall events (e.g. Marvin & Asner, 2016). Airborne Lidar data can bridge the scale gap between field-based measurements and satellite observations by collecting three-dimensional information on forest structure over large areas (Asner *et al.*, 2013; Espírito-Santo *et al.*, 2014; Hunter *et al.*, 2015). Repeat Lidar measurements of the same forest areas provide unprecedented detail regarding changes in the forest canopy over time (Kellner *et al.*, 2009; Andersen *et al.*, 2014; Hunter *et al.*, 2015; Réjou-Méchain *et al.*, 2015; Marvin & Asner, 2016), leading to a better understanding of the processes governing canopy turnover and the associated carbon fluxes. However, Lidar data may not provide definitive evidence for the mechanisms that contribute to carbon loss from canopy turnover, including branch fall, tree fall and multiple tree fall disturbances. A combination of field measurements and repeat Lidar data may

therefore advance our mechanistic understanding of canopy turnover and carbon cycling in Amazon forests beyond the use of Lidar data alone (e.g., Marvin & Asner, 2016).

Drought impacts on Amazon forest structure depend on the severity and duration of rainfall deficits. In the short term, soil water deficits trigger an increase in stomatal closure and leaf abscission (Brando et al., 2007, 2014), thereby reducing net primary productivity during drought conditions (Feldpausch et al., 2016; but see Doughty et al., 2015). With increasing drought severity, both empirical and experimental studies indicate a positive relationship between drought severity and mortality rates in Amazon forests (Nepstad et al., 2007; Phillips et al., 2009, 2010; da Costa et al., 2010). The timing of mortality responses to drought is uncertain, however. During the 1997–1998 El Niño drought, Williamson et al. (2000) observed a 71% increase in mortality, but this increase was restricted to the drought year (1997). Other long-term plot data also show a single-year increase in mortality from droughts across the southern Amazon in 2007 (Brando et al., 2014) and 2010 (Doughty et al., 2015). By contrast, experimental studies suggest a delay between drought and tree mortality, especially for large trees, with a peak in mortality following 3 yr of experimental throughfall exclusion (Nepstad et al., 2007; da Costa et al., 2010). In these circumstances, tissue damage from hydraulic failure may weaken but not immediately kill canopy trees (Rowland et al., 2015). Drought responses are also species-specific; trees with lower water use efficiency are particularly prone to drought-induced mortality (e.g. Phillips et al., 2009; Feldpausch et al., 2016), a trait common to pioneer species found in greater abundance in canopy gaps, edges, and secondary or degraded forests.

Branch losses may also contribute to long-term changes in forest structure and productivity following drought conditions, but previous studies provide few constraints on the spatial and temporal variability in branch loss (Palace et al., 2008). Coarse woody debris (CWD) from branch and tree falls increased following drought in the central Brazilian Amazon (Rice et al., 2004; Brando et al., 2007), yet plots in the Bolivian Amazon showed no increase in branch loss following the 2010 drought (Doughty et al., 2015). In part, these differences may reflect underlying regional patterns of branch loss, as documented across the western Amazon by Marvin & Asner (2016) in the absence of drought conditions. Pulses of drought-induced mortality and branch loss have pronounced impacts on neighbouring trees, with both physical impacts from collateral damage and physiological implications based on the reduction in competition for light and water among surviving individuals (da Costa et al., 2018). Repeat airborne Lidar data offer the potential to advance our understanding of regional-scale patterns of canopy tree and branch turnover during drought periods.

In this study, we characterized canopy turnover during average and drought years in the central Brazilian Amazon using a time series of high-density, small-footprint airborne Lidar data. Lidar data from 2013, 2014 and 2016 captured turnover dynamics before and immediately following the 2015–2016 El Niño drought across intact and fragmented forests near Santarém, Pará. Field surveys of tree mortality and CWD within canopy turnover

events were conducted shortly after the third Lidar collection in 2016 to quantify carbon losses associated with canopy turnover from branch fall, tree fall and collateral damage to understory vegetation. Combined, Lidar and field data provided estimates of the spatial and temporal variability in canopy turnover and associated carbon fluxes from the above-ground biomass to coarse woody debris pools. Our study specifically addressed the following four questions: (1) How do canopy turnover rates compare between intact and fragmented forests? (2) What are the contributions from branch fall, tree fall and multiple tree-fall events to total canopy turnover? (3) Do average turnover rates in Amazon forests increase during drought events? (4) What are the carbon consequences, measured as CWD, of canopy turnover in Amazon forests? These analyses offer a critical look at the individual tree and landscape-scale responses to drought conditions identified by rainfall exclusion experiments (Nepstad et al., 2007; da Costa et al., 2010; Rowland et al., 2015) and inventory plots (e.g. Phillips et al., 2010; Feldpausch et al., 2016).
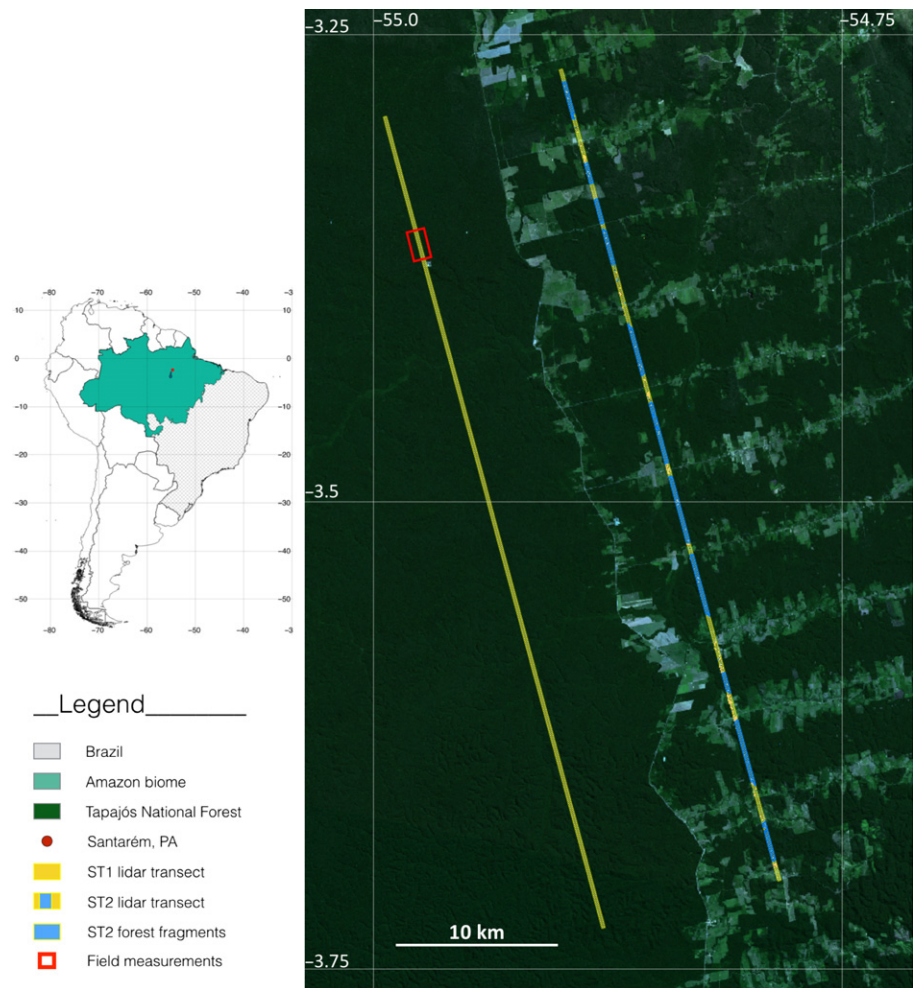
Materials and Methods

Precipitation data

Satellite and meteorological station data suggest that 2015 and 2016 were the driest years since 2001 for the Tapajós National Forest (TNF) region near Santarém, Pará (Fig. 1, Supporting Information Fig. S1). Based on data from NASA's Tropical Rainfall Measurement Mission (TRMM, monthly 0.25° data product TMPA/3B43, v.7), mean annual precipitation for the TNF region was 2054 mm yr^{-1} during 2001–2016 (TRMM, 2011). Estimated precipitation was average or above average in 2013 (2342 mm) and 2014 (2000 mm), whereas total precipitation was below average in both 2015 (1533 mm) and 2016 (1862 mm). Maximum cumulative water deficit (MCWD; Aragão et al., 2007) peaked in 2015 (−431 mm) compared to the average annual MCWD for 2001–2016 (−233 mm). Station data from Brazil's National Meteorological Institute (Instituto Nacional de Meteorologia, INMET) station 25 km north of the TNF in Belterra, Pará (−2.63°, −54.95°), provide a similar estimate for the MCWD in 2015 (−478 mm, Fig. S1).

Airborne Lidar data

Lidar data were collected over intact and fragmented forests in the central Brazilian Amazon near the city of Santarém, Pará (see Fig. 1). Data were acquired along two 50 km parallel transects (200 m width, 995 ha area) in September 2013 (t1), June 2014 (t2) and March 2016 (t3). The time intervals between Lidar collections were 0.75 yr (t1–t2) and 1.83 yr (t2–t3). The ST1 transect covered a section of intact old-growth terra firme forest within the TNF. The ST2 transect paralleled the ST1 transect on the opposite side of the BR-163 highway and covered a range of different land cover types. Analysis of ST2 data was restricted to 12 forest fragments, ranging in size from 23.5 to 80 ha (Table 1). Lidar data were collected with very high average return densities: 9.2–10.8 points per m^2 (ppm^2) in 2013, 39.6–59.9 ppm^2 in

Fig. 1 Study area in the central Brazilian Amazon near Santarém, Pará, with repeat Lidar collections over intact (ST1, yellow) and fragmented (ST2, blue) forest areas. Lidar data were acquired for transects of 50 km × 0.2 km in 2013, 2014 and 2016, and field measurements of coarse woody debris in canopy turnover areas were conducted in 2016 within a 20 ha subset of ST1 (red outline). The underlying Landsat 8 imagery (30 June 2016) depicts closed-canopy Amazon forests in green and deforested areas for agricultural uses in light green and blue.

Legend
- Brazil
- Amazon biome
- Tapajós National Forest
- Santarém, PA
- ST1 lidar transect
- ST2 lidar transect
- ST2 forest fragments
- Field measurements

2014 and 29.3–33.9 ppm^2 in 2016. Higher point densities in the second and third Lidar collections provided robust estimates of canopy changes based on the increased likelihood of detecting residual canopy material in turnover areas. Data in the first two surveys were collected with an Optech ALTM Orion laser scanner at 853 m average flight altitude, 11° field of view and 65% flight line overlap. The third survey used an Optech ALTM 3100 laser scanner at 650 m average flight altitude, 15° field of view and 70% flight line overlap. Lidar data in this study are available online from the Sustainable Landscapes Brazil Project (https://www.paisagenslidar.cnptia.embrapa.br/webgis/).

Lidar return data from the three collections were merged to generate a single digital terrain model (DTM) to normalize estimated heights of vegetation returns from t1, t2 and t3 data (Hunter *et al.*, 2013). Ground returns were classified using a progressive morphological filter (Zhang *et al.*, 2003). Delaunay triangulation was used to create a Triangulated Irregular Network (TIN) of ground hits, and DTM elevations on a 1 m raster grid were linearly interpolated from the TIN surface (Cook *et al.*, 2013). Canopy height models (CHMs) at 0.5 m spatial resolution were then generated separately for t1, t2 and t3 following Cook *et al.* (2013) by interpolating canopy height values from a 0.5 m TIN surface created from the greatest return height in

every 0.5 m grid cell. Canopy turnover events were identified based on contiguous clusters ($\geq 4\,m^2$) with ≥ 3 m height losses between Lidar collections (Fig. 2). Turnover events were analyzed based on the projected area (m^2) and change in canopy volume (m^3) between 0.5 m CHM layers for each data collection, with annualized estimates of the number and area of turnover events in each study region ($ha^{-1}\,yr^{-1}$) based on the time interval between Lidar collections.

Lidar data from both transects were subdivided to investigate latitudinal gradients in canopy turnover. The ST1 transect over intact forests was divided into five subsections (ST1a, b, c, d and e) to evaluate north–south gradients in forest structure and topography (Table 1). On the opposite side of the highway, land cover types within the ST2 transect were evaluated based on contemporary Landsat 8 surface reflectance imagery (Path 227 Row 062, Date 2016-June-30, Source: USGS Earth Explorer, http://earthexplorer.usgs.gov/) as well as Lidar return distributions and canopy height information. We identified 12 fragments of contiguous forest area with Lidar-derived canopy cover $\geq 10\%$, mean canopy height ≥ 20 m and forest patch width ≥ 20 m (see Fig. 1). Forest fragments were labeled from north to south as FR01 to FR12, and individual fragments ranged in size from 23.5 to 80.0 ha (562 ha total area, see Table 1).

Table 1 Canopy structure, terrain variability and turnover dynamics derived from repeat Lidar over intact (ST1) and fragmented (ST2) Amazon forests

Transect	Segment/ fragment	Area (ha)	Elevation (m, min–max)	Terrain slope (degrees, μ ± σ)	2016 Canopy heigh (m, μ ± σ)	CH Skew-ness	Turnover 2013–2014 (% yr⁻¹)	Turnover 2014–2016 (% yr⁻¹)	% Δ Turn-over (%)	2013–2014 events (no. ha⁻¹ yr⁻¹)	2014–2016 events (no. ha⁻¹ yr⁻¹)	2013–2014 mean size (ha)	2014–2016 mean size (ha)
ST1	ST1a	171.2	102–209	4.7 ± 4.4	29.3 ± 10.4	−0.389	1.89	3.15	66.3	6.5	10.8	28.9	29.3
	ST1b	206.0	60–148	5.3 ± 4.8	25.8 ± 8.7	−0.111	1.73	3.13	80.9	5.6	11.4	30.7	27.5
	ST1c	206.0	91–192	5.5 ± 4.9	26.9 ± 9.3	−0.218	1.68	3.49	107.4	6.0	10.4	27.8	27.7
	ST1d	206.0	80–209	13.8 ± 10.1	27.1 ± 8.3	−0.117	1.80	2.77	54.0	6.3	8.9	28.4	29.4
	ST1e	167.0	99–257	17.9 ± 7.9	28.8 ± 9.2	−0.155	1.87	2.51	34.2	6.9	8.1	26.9	30.8
ST2	FR01	42.7	76–139	7.6 ± 6.4	26.6 ± 8.1	0.074	1.58	3.46	119.2	5.7	12	27.5	28.9
	FR02	24.3	84–161	11.0 ± 7.1	24.9 ± 7.2	−0.183	1.65	3.98	141.2	5.9	11.7	27.9	34.1
	FR03	29.7	112–136	2.9 ± 1.6	23.8 ± 7.7	−0.211	1.68	3.30	96.8	6	12.1	27.9	27.3
	FR04	42.1	102–144	3.8 ± 2.4	24.9 ± 8.6	−0.328	1.90	3.35	76.3	6.8	10.7	28.1	31.3
	FR05	58.4	66–151	5.5 ± 6.5	21.8 ± 9.2	0.534	2.46	4.70	91.1	11.1	17	22.1	27.6
	FR06	26.6	88–148	4.5 ± 2.7	23.1 ± 8.6	0.289	2.45	3.66	49.4	10.1	13.9	24.2	26.3
	FR07	42.8	57–107	5.3 ± 6.4	24.0 ± 7.4	−0.082	1.36	2.07	52.3	5.5	9.7	24.8	21.4
	FR08	80.0	59–115	6.6 ± 6.5	24.0 ± 8.0	−0.274	1.62	2.73	68.2	6.1	8.4	26.4	32.4
	FR09	73.5	71–140	11.0 ± 10.0	25.0 ± 7.8	−0.513	2.07	2.17	4.9	8.4	7.9	24.6	27.4
	FR10	23.5	74–125	10.0 ± 10.2	26.0 ± 8.2	−0.031	1.73	2.21	27.7	5.1	8	34.3	27.8
	FR11	76.0	80–205	14.0 ± 10.2	25.4 ± 8.3	−0.156	2.16	2.80	29.3	8.7	8.8	25.0	31.8
	FR12	41.9	115–217	13.9 ± 8.2	25.1 ± 10.2	0.141	3.06	3.03	−0.8	11.7	10.7	26.2	28.4

Coarse woody debris measurements

Ground-based measurements of CWD were collected in July 2016 within a 20 ha area of the ST1 airborne Lidar coverage in the TNF (see Fig. 1). The objective of the field survey was to map and measure downed trees and branches in canopy turnover events that were identified using the 2014 and 2016 Lidar canopy height models (Fig. 2). A high-precision Trimble Geo7X GPS rover with external antenna was used to navigate to the ground location of 78 different canopy turnover areas. Within each area, the location and size of all downed trees (diameter at breast height (DBH), height) and branches (in segments; diameter at both ends (≥ 1 cm), segment length) were measured and the turnover event was classified according to the nature of the disturbance (branch, tree, multiple tree fall), physical mechanism of turnover (uprooted, snapped, broken) and the decay class of the wood (1–5 from least decayed to most decayed, following Keller *et al.*, 2004). Measurements within each turnover area were used to estimate carbon losses associated with branch fall, tree fall and multiple tree fall events and to evaluate predictive relationships between canopy turnover and carbon losses using Lidar metrics. Additionally, whole-tree measurements of CWD ($n = 18$) from tree fall and multiple tree fall turnover areas were compared to existing allometric equations for above-ground biomass (AGB) in tropical forest trees (see Table S1).

The total mass of downed woody material in each field-measured turnover area was estimated using field measurements of CWD (Table S2). Branch mass was calculated using the volume equation of a truncated cone (assuming circular cross-sections) and a site-level average wood density established for the TNF ($0.64\ \mathrm{g\ cm^{-3}}$, Hunter *et al.*, 2013). Tree mass was calculated using Chave's Model I moist forest allometry, which is based on tree DBH, total tree height and wood density (Chave *et al.*, 2005). For each of the 78 turnover areas, we calculated the total amount of CWD measured within the turnover area and compared field-based estimates of biomass change with different Lidar-derived metrics of canopy changes between 2014 and 2016, including the projected area of canopy turnover events and the change in canopy volume between 2014 and 2016 CHM layers at 0.5 m resolution. For comparison, we also estimated biomass change using a Lidar–biomass model developed using mean top of canopy height (TCH) at 0.25 ha resolution (Longo *et al.*, 2016). Simulations considered biomass changes using only height losses from canopy turnover (Marvin & Asner, 2016) and both losses and gains in canopy height between 2014 and 2016 for 0.25 ha grid cells with CWD measurements for > 75% of canopy turnover area ($n = 13$).

Relationships between field measurements of CWD and Lidar metrics were used to estimate total carbon losses from canopy turnover in the ST1 transect under two scenarios. In the first, all canopy turnover was considered branch fall to provide a conservative estimate of carbon losses using the relationship between canopy volume change (m³) and CWD production from single branch fall events. In a second scenario, we used the distribution of Lidar-derived changes in canopy volume from field-measured turnover events to separate branch fall (≤ 100 m³), single tree fall
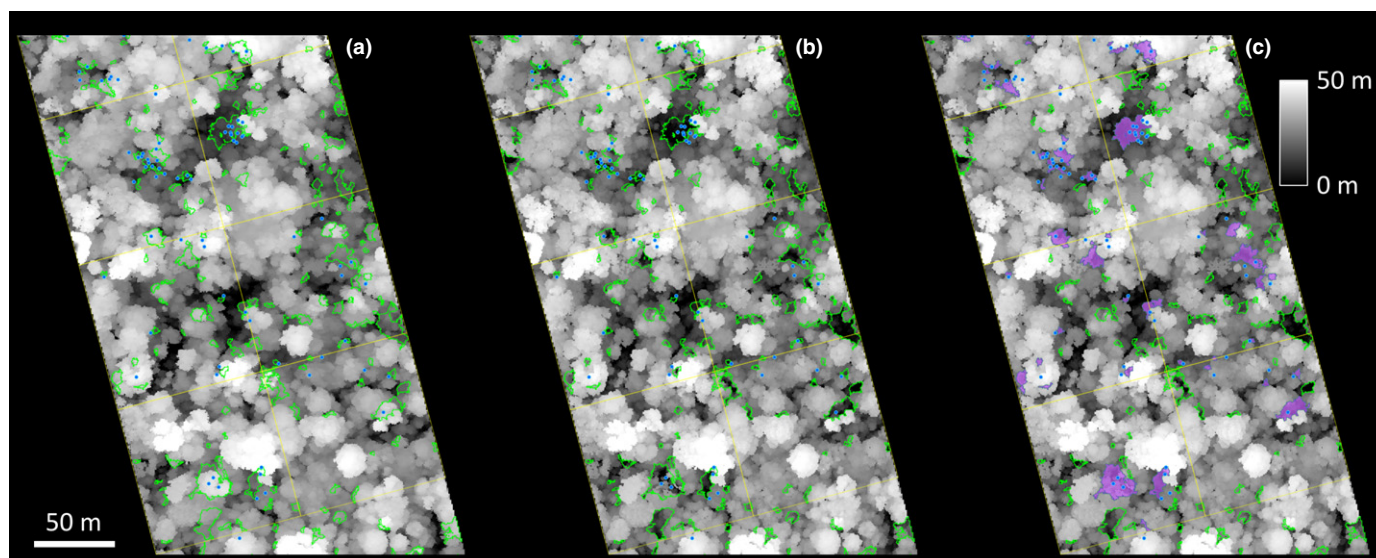
Fig. 2 An 8 ha subset of the ST1 transect showing canopy turnover events (green outlines) between 2014 (a) and 2016 (b) 0.5 m resolution Lidar canopy height models (CHMs). (c) Turnover events mapped in the field are shaded purple, and blue dots indicate stem locations for tree fall and multiple tree fall turnover events, including both canopy and understory trees.

or multiple branch fall (100–500 m^3), and multiple tree fall events (≥ 500 m^3). Intermediate-sized changes were randomly assigned with equal probability to either single tree fall or multiple branch fall categories to estimate carbon losses.

Results

Forest structure

Parallel Lidar transects in this study captured similar variability in terrain elevation and forest characteristics inside and outside the TNF (Table 1). Terrain elevation varied between 50 and 250 m asl and slope followed a north–south gradient, with more steeply sloped terrain in the southern sections (13.4° mean slope, STd-e and FR09-12) than northern portions of the transects (5.2° mean slope, STa-c and FR01-08). The distribution of canopy heights along the ST1 transect was consistent among segments, with little variation in mean canopy heights. On average, ST2 fragments were shorter than intact forests (24.5 m vs 27.8 m). Canopy height distributions were similar for intact ST1 segments and most forest fragments in ST2, with tall, closed-canopy profiles (see Table 1). Four of the ST2 fragments (FR01, 05, 06 and 12) had more open canopy profiles, with skewed canopy height distributions that may indicate a history of disturbance from selective logging or understory fires before the initial Lidar collection in 2013 (Longo *et al.*, 2016).

Turnover dynamics

The area of canopy turnover was 65% higher, on average, in the second interval for both intact and fragmented forests. Annualized rates of canopy turnover for intact forest segments increased from 1.68–1.89% yr^{-1} (mean 1.79% yr^{-1}) in 2013–2014 to 2.51–3.49% yr^{-1} (mean 3.01% yr^{-1}) between 2014–2016

(Table 1). All five ST1 segments had higher turnover in 2014–2016, with greatest increases in ST1c (107.4%) and ST1b (81.2%). The range of annualized turnover during each interval was larger for forest fragments of ST2, but turnover rates also increased between the first (1.36–3.06% yr^{-1}, mean 1.98% yr^{-1}) and second time intervals (2.17–4.70% yr^{-1}, mean 3.12% yr^{-1}). Individual forest fragments in the ST2 transect had more variable increases in canopy turnover between 2013–2014 and 2014–2016; turnover more than doubled in FR01 and FR02, nearly doubled in FR03 and FR05, while turnover rates in FR09 increased only slightly (4.9%) and turnover in FR12 was 0.8% lower in the second interval (Table 1).

Increases in turnover between 2013–2014 and 2014–2016 showed a strong north–south gradient (Fig. 3a). Terrain slope contributed to the observed north–south gradient in canopy turnover (Fig. 3b), with larger increases observed in the flatter, northern areas of the study and smaller increases in the southern sections of each transect with more variable terrain. However, broad patterns of terrain variability were not preserved at the scale of individual turnover events; the distributions of terrain slope within areas of canopy turnover were consistent between time intervals, with no evidence that canopy turnover from branch or tree fall events was more likely on steeper slopes in either time interval.

The average number of turnover events increased between time periods, but the mean size of canopy changes was similar for both intervals (Table 1). The density of canopy turnover events increased from 6.3 to 10.0 events ha^{-1} yr^{-1} in intact forest segments of ST1 and from 7.6 to 10.9 events ha^{-1} yr^{-1} in fragmented forest areas along ST2. The average size of turnover events remained relatively constant in the intact forest segments (28.5 m^2 in t1–t2 vs 28.7 m^2 in t2–t3) and increased slightly in the forest fragments (from 26.6 m^2 in t1–t2 to 28.7 m^2 in t2–t3).
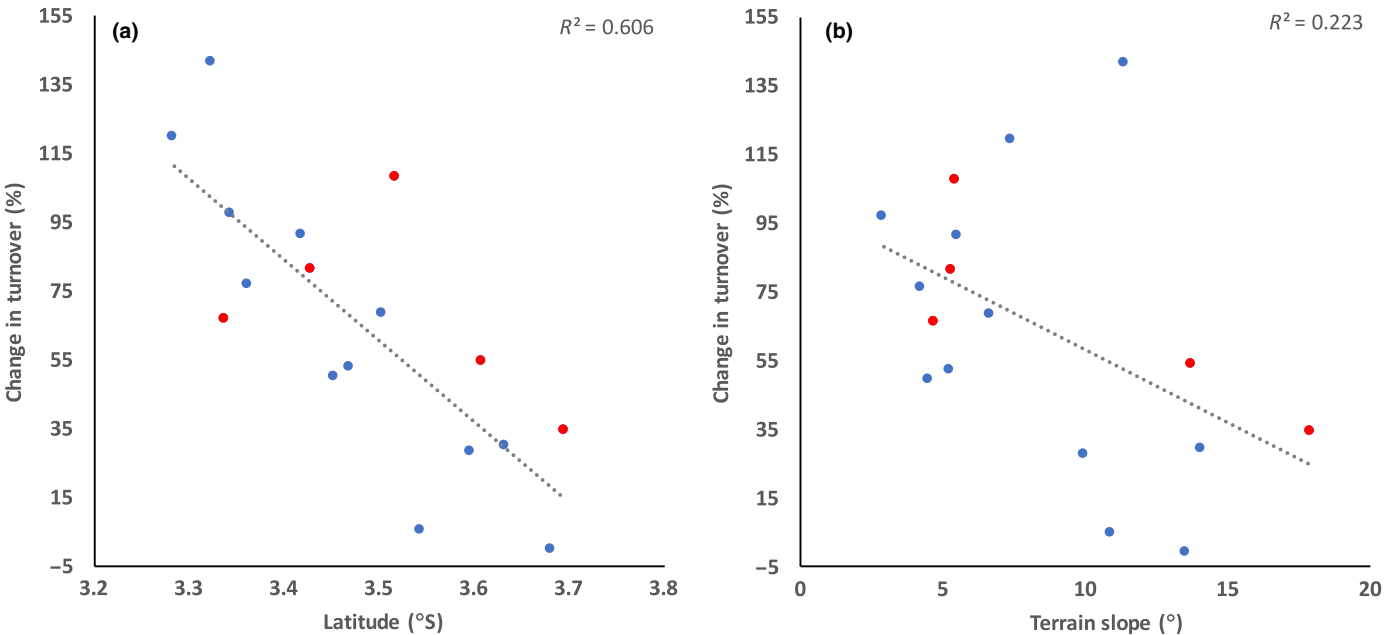
Fig. 3 Increases in annualized canopy turnover rates between 2013–2014 and 2014–2016 varied by latitude (a) and terrain slope (b) across intact (red) and fragmented forests (blue).

Canopy turnover events were classified into different size categories based on break points in field measurements (Table 2; Fig. 4). Across both intact and fragmented forests, c. 75% of turnover events were small (< 25 m²), c. 20% were intermediate (25–100 m²) and c. 5% were large (> 100 m²). Large turnover events accounted for the largest fraction of the total turnover area (40%), with smaller contributions from intermediate (32%) and small (28%) turnover events. Differences in the observed proportions between time intervals were small (< 2.7%). Examining all study areas, no clear pattern emerged in the size distributions of turnover events between 2013–2014 and 2014–2016.

Similarly, there was no consistent evidence that taller trees contributed a greater proportion of canopy turnover during the interval (2014–2016) that included the strong El Niño drought. The distribution of initial maximum canopy heights within the turnover events in the 2013–2014 and 2014–2016 intervals were largely consistent (Fig. S2). Within the intact forest transect

(Fig. S2a), only subsections ST1a and ST1d showed a positive shift in the initial maximum height distributions (Kolmogorov–Smirnov test, $P < 0.001$ in both segments). Among the forest fragments (Fig. S2b), only FR02 and FR09 showed a statistically significant increase in initial maximum height distributions (Kolmogorov–Smirnov test, $P < 0.018$ in both fragments).

Coarse woody debris (CWD)

CWD was measured in 78 canopy turnover events within the ST1 Lidar transect in 2016 (see Fig. 1). In the field, canopy turnover was classified as single branch fall ($n = 20$), multiple branch fall ($n = 14$), single tree fall ($n = 16$) and multiple tree fall ($n = 28$). Based on the area of canopy turnover estimated from repeat Lidar, single branch falls were the smallest in size (11.3 m² on average) and multiple tree falls were the largest (101.1 m² on average), whereas multiple branch falls and single tree falls had

Table 2 Summary of canopy turnover events from repeat Lidar measurements and field surveys of coarse woody debris

Canopy turnover events	Count	Canopy height (m) 2014 mean	2016 mean	Δ Area (m²) Min	Max	Mean	SD	Δ Volume (m³) Min	Max	Mean	SD	Δ Biomass (kg) Min	Max	Mean	SD
Branch fall – single	20	34.7	25.6	4.0	21.3	11.3	4.5	25.4	346.5	110.7	79.3	2.9	432.6	58.8	91.1
Branch fall – multiple	14	33.6	24.4	4.0	108.8	23.6	26.5	15.2	1808.0	270.5	434.4	8.1	1347.2	261.9	384.6
Tree fall – single	16	25.0	13.3	5.25	47.8	16.0	12.0	51.2	638.4	194.2	186.4	43.4	1048.2	312.7	301.8
Tree fall – multiple	28	27.7	16.0	7.0	370.3	101.1	102.8	66.8	6171.2	1397.1	1676.1	40.3	12938.6	2014.8	2905.5
All events	78	30.0	19.4			46.7	74.5			618.3	1171.4			849.5	1945.2

Turnover events were classified as branch fall, multiple branch fall, tree fall and multiple tree fall based on field surveys. Changes in canopy area and canopy volume were derived from differences between the 2014 and 2016 Lidar surveys; biomass change by turnover event class was estimated using field measurements.
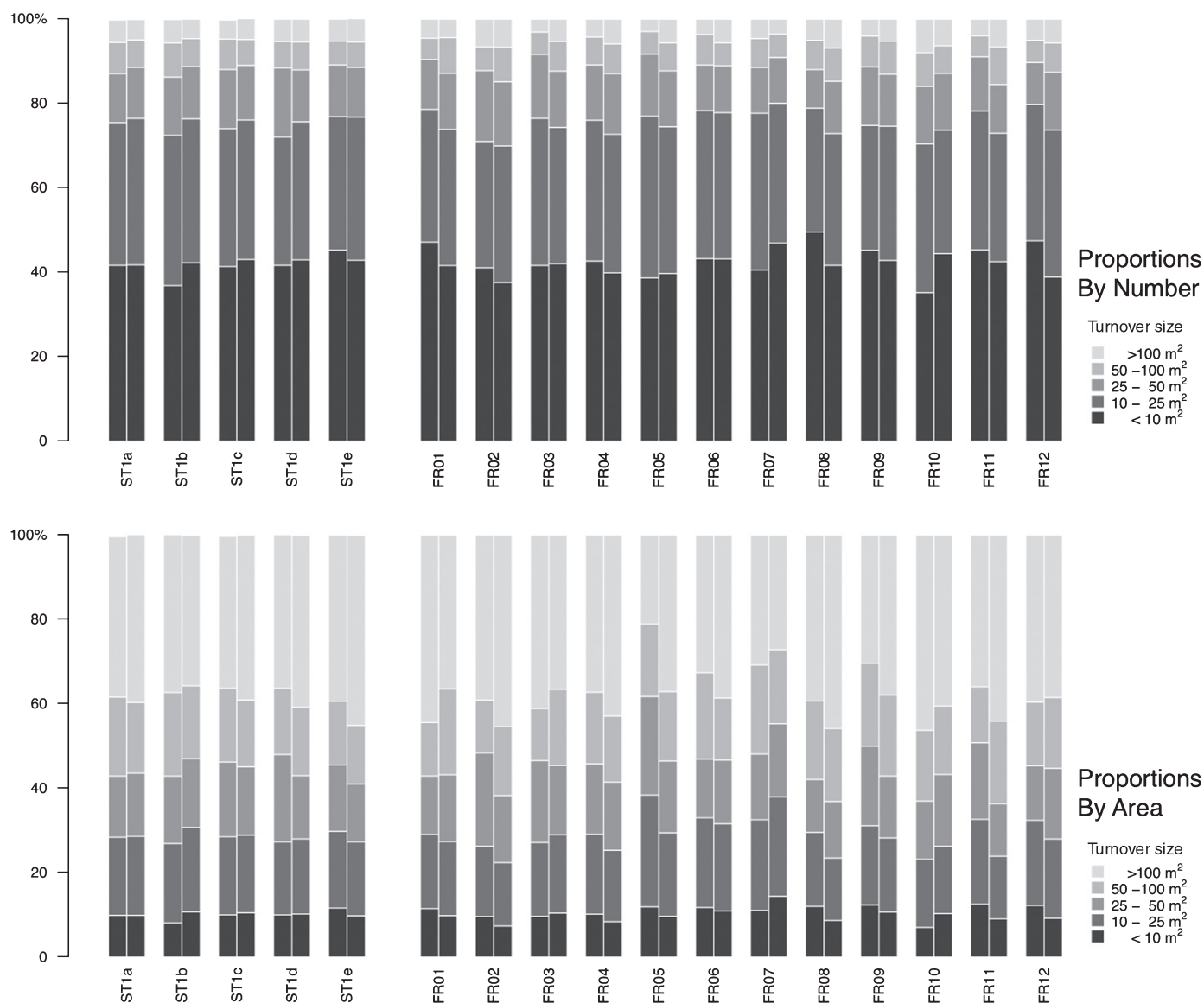
Fig. 4 Total canopy turnover increased between 2013–2014 and 2014–2016, but the proportions of canopy turnover events (upper panel) and total turnover area (lower panel) by size class in intact (ST1a–e) and fragmented (FR01–12) forest areas were consistent between 2013–2014 (left bar) and 2014–2016 (right bar).

overlapping distributions of Lidar-derived turnover size and changes in canopy volume (Table 2). Accordingly, the amount of CWD measured in locations of single branch falls was the smallest (mean 59 kg), and multiple tree fall events represented the largest amount biomass change from canopy trees and collateral damage to understory vegetation (mean 2015 kg CWD). The two intermediate classes corresponding to multiple branch falls or single tree falls generated similar amounts of CWD despite different underlying turnover mechanisms. Changes in canopy area and volume were actually larger for multiple branch fall than for single tree fall events, on average, despite lower mean biomass losses (Table 2).

CWD measurements for whole trees within turnover events ($n = 18$) complement existing destructive harvest studies of tropical forest allometry. Whole tree measurements of CWD were compared to existing allometries for tropical forest trees from Chave *et al.* (2005) and Feldpausch *et al.* (2012), using site-specific parameters for tree height and wood density from Hunter *et al.* (2013) (Tables S1, S2). On average, tree stems contained 67.2% of woody biomass, with a mean of 32.8% of woody biomass held in the crown. This 2 : 1 ratio is similar to previous measurements in the central Amazon (Higuchi *et al.*, 1998). Although most trees had a larger proportion of their mass in the stem than in the crown, only a few individuals conformed to the 2 : 1 average ratio (Table S2). Two individuals had much heavier crowns than stems (70% vs 30%, respectively), and an additional five trees had crowns and stems of comparable mass. The range of stem : crown biomass ratio highlights the potential for branch loss to decrease AGB of canopy trees before tree death.

Estimates of AGB from tropical tree allometries were very sensitive to height estimates. In general, allometric equations using existing diameter–height relationships overestimated the field-measured tree biomass as CWD (Table S1), with only four trees where the modeled AGB estimate was lower than field measurements of CWD (Fig. S3). Incorporating a local calibration of the diameter–height relationship (Hunter *et al.*, 2013) into the allometric equations resulted in lower root mean square error values and a higher R^2 between measured (CWD) and modeled AGB (see Table S1), but using field measurements of tree height in the allometric models resulted in the smallest mean relative error with both the Chave *et al.* (2005) (14.9%) and the Feldpausch *et al.* (2012) allometries (12.1%).

CWD from canopy turnover

Changes in canopy height, area and volume were weakly correlated with total carbon losses from branch fall, tree fall and multiple tree fall events. The modest relationships between biomass and canopy volume changes reflected the wide range of canopy expressions for branch and tree fall events in tall, multi-layered Amazon forests (Fig. 5). Separating Lidar–biomass relationships by mechanism provided further evidence for the complexity of CWD production from canopy and understory vegetation from different turnover classes (Fig. 5b–e). In all four categories of canopy turnover, the largest field-measured CWD from canopy turnover generated small changes in canopy volume from repeat Lidar acquisitions (Fig. 5b–e). In addition, the slope of the

relationships between field-measured CWD and Lidar-based estimates of canopy volume change varied by more than a factor of 2 between CWD production from single branch (0.388, $R^2 = 0.24$) and single tree fall events (0.402, $R^2 = 0.19$) and multiple branch (0.903, $R^2 = 0.31$) and multiple tree fall events (0.882, $R^2 = 0.30$). In all cases, the slope ($\pm$ SE) differed from the relationship between Lidar-derived canopy volume and biomass at 0.25 ha resolution using the model developed for TCH from Longo *et al.* (2016).

Estimated CWD production in the ST1 transect increased proportionally to canopy turnover between 2014–2016 and 2013–2014 (Fig. 6). Assuming all turnover events were a result of branch fall (see Fig. 5e) generated a conservative estimate of a 63% increase in annualized CWD production from 0.38 to 0.61 Mg C ha^{-1} yr^{-1}. Using turnover size to assign events to branch, treefall and multiple tree fall classes increased the estimated CWD production during the drought period by 62%, from 0.76 Mg C ha^{-1} yr^{-1} in 2013–2014 to 1.22 Mg C ha^{-1} yr^{-1} in 2014–2016. Importantly, large turnover events classified as single or multiple tree falls accounted for 81.7% and 80.3% of estimated carbon losses from canopy turnover in 2013–2014 and 2014–2016, respectively.

The relationship between field measurements and Lidar-derived estimates of biomass change between 2014 and 2016 was also variable at 0.25 ha resolution (Fig. 7). The Marvin & Asner (2016) approach using only canopy height losses to quantify biomass change overestimated CWD production from field measurements in all but one 0.25 ha grid cell (Fig. 7a). By contrast,
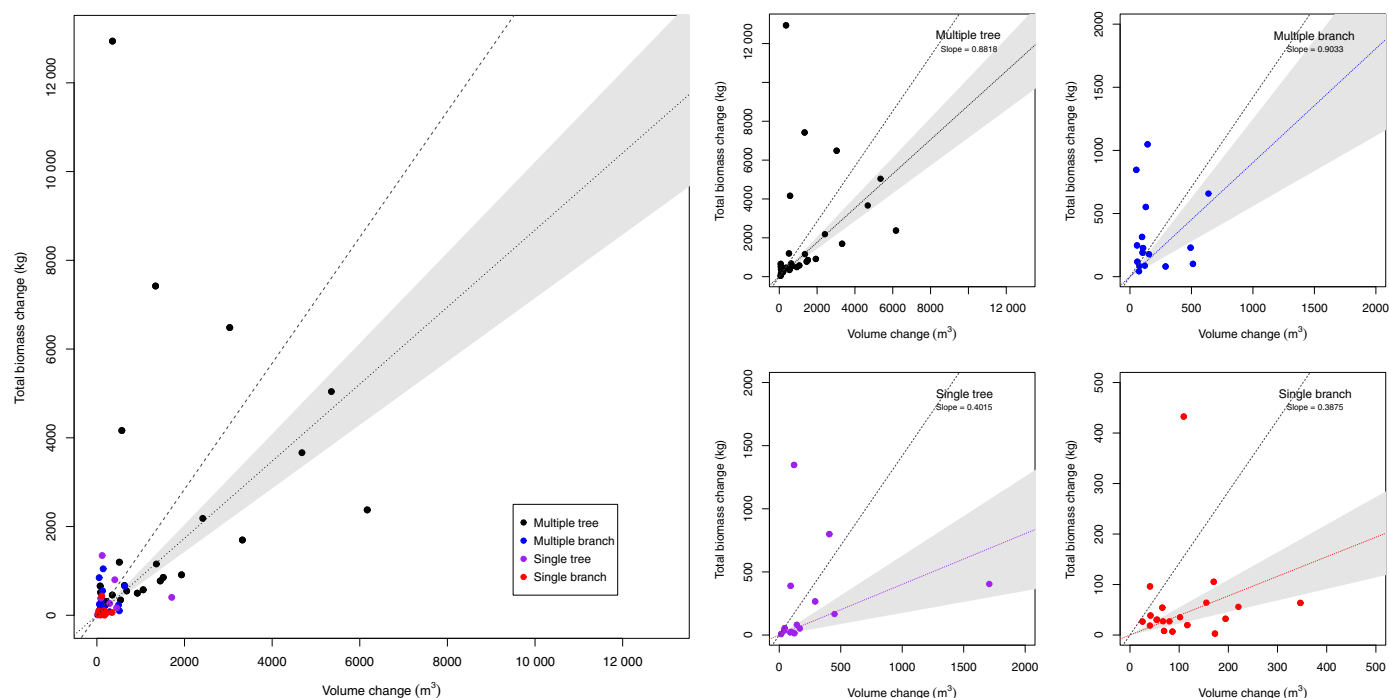

Fig. 5 Lidar–biomass relationships within canopy turnover events varied by turnover class. Dotted lines indicate the regression relationship between the Lidar-based change in canopy volume (m^3) and field-measured biomass change, and the standard error of the regression slope is indicated with grey shading. The grey dashed line shows the average Lidar canopy volume–biomass relationship at 0.25 ha resolution for the ST1a transect following Longo *et al.* (2016).
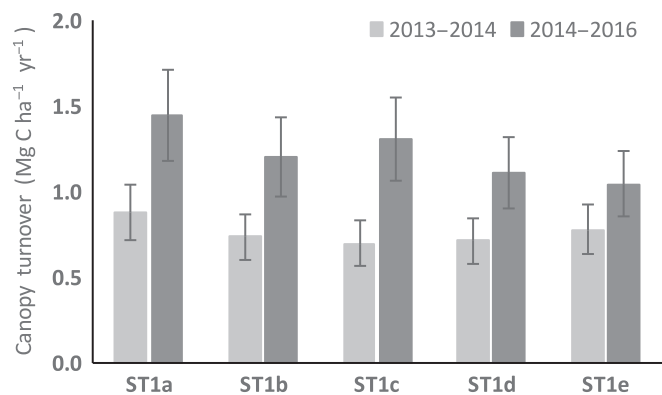
Fig. 6 Annualized carbon losses from canopy turnover in intact forests areas of ST1 during 2013–2014 and 2014–2016. Turnover areas were classified based on Lidar-derived changes in canopy volume, and coarse woody debris (CWD) production from branch and tree fall events was estimated using relationships between Lidar-derived changes in canopy volume and CWD measurements (see Fig. 5). The standard error of the regression slope was used to propagate uncertainty associated with carbon loss as CWD from individual turnover events.

the net difference in estimated AGB using both gains and losses in canopy height between 2014 and 2016 was closer to the 1 : 1 line, particularly for 0.25 ha cells with larger field-based losses, whereas small CWD losses measured in the field were offset by net gains in canopy height between 2014 and 2016 (Fig. 7b). Differences at both the scale of individual turnover events and 0.25 ha resolution underline the challenge of estimating small

changes in canopy and understory forest carbon stocks using multi-date Lidar.

Discussion

Repeat, high-density airborne Lidar data provide a unique canopy perspective on the response of Amazon forests to drought. In the central Brazilian Amazon, intact and fragmented forests responded similarly to interannual variability in climate conditions, with comparable increases in canopy turnover during the 2015–2016 El Niño drought period in both intact (+70.1%) and fragmented forests (+57.2%). Overall, estimated CWD from canopy turnover increased by 62% during the drought period, averaging $1.22 \, \mathrm{Mg \, C \, ha^{-1} \, yr^{-1}}$ in 2014–2016. The observed increases in canopy turnover and associated carbon losses are consistent with reports of elevated tree mortality during Amazon droughts from forest inventory plots (e.g. Williamson et al., 2000; Phillips et al., 2009; Brienen et al., 2015; Feldpausch et al., 2016), yet the canopy perspective and regional sampling possible with airborne Lidar expand our understanding of forest dynamics beyond the plot scale. Branch fall events were ubiquitous across all forests in both study periods, but sub-lethal canopy changes accounted for only c. 30% of canopy turnover area and c. 20% of estimated CWD production from canopy and understory trees. These results differ from a previous report of greater turnover area and carbon losses from 'upper canopy gaps' associated with branch fall compared with 'full canopy gaps' from tree fall events in the Colombian and Peruvian Amazon (Marvin & Asner,
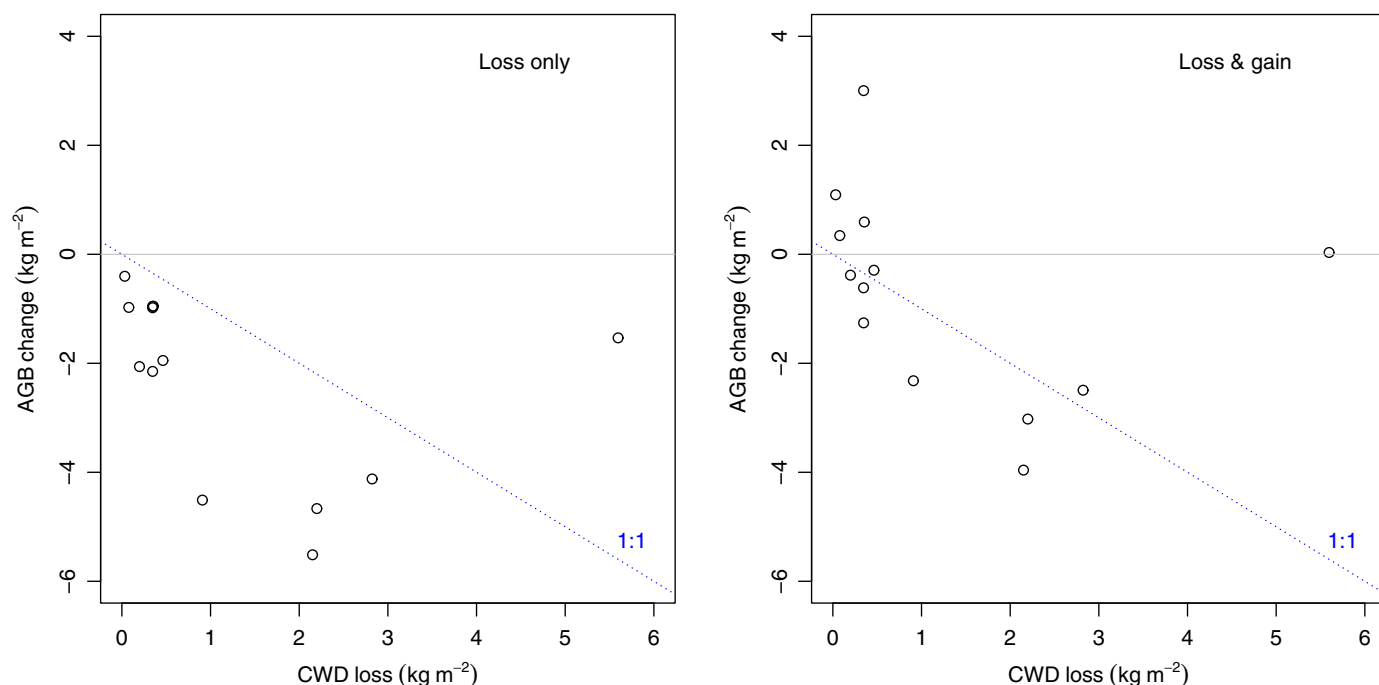

Fig. 7 Estimated changes in above-ground biomass (AGB) from field measurements of canopy turnover between 2014 and 2016 and modeled biomass change from Lidar data at 0.25 ha resolution. The analysis was restricted to 0.25 ha grid cells with > 75% of turnover area measured in the field ($n = 13$, mean = 88%). AGB in 2014 and 2016 was estimated using the biomass model developed by Longo et al. (2016) based on top-of-canopy height. The left panel uses only canopy height losses within turnover areas (following Marvin & Asner, 2016), while the right panel includes both canopy height losses and gains between the 2014 and 2016 Lidar acquisitions to estimate changes in AGB. CWD, coarse woody debris.

2016). Even over shorter length scales (≤ 50 km), repeat Lidar surveys captured landscape-scale dynamics in forest turnover, including a strong north–south gradient in the relative increase in canopy turnover during the drought interval. Underlying drivers of variability in Amazon forest dynamics remain an important area for further study, including regional gradients in forest structure (Simard *et al.*, 2011), composition (Fauset *et al.*, 2015; Feldpausch *et al.*, 2016), and drought frequency and severity (e.g. Phillips *et al.*, 2009; Lewis *et al.*, 2011).

Mechanisms of canopy turnover

Canopy turnover results in this study differed from findings in simulated drought experiments. Previous studies reported an increase in mortality of large trees following multiple years of partial throughfall exclusion (Nepstad *et al.*, 2007; da Costa *et al.*, 2010; Rowland *et al.*, 2015). By contrast, increased turnover in 2014–2016 relative to 2013–2014 came from all size classes, not only from large tree fall or multiple tree fall events, and the distributions of tree heights and turnover sizes were similar in both time periods. Lidar-based assessments of canopy turnover were therefore more similar to plot studies showing short-term increases in mortality rates across a range of size classes (Williamson *et al.*, 2000; Doughty *et al.*, 2015). Additional Lidar surveys of the region would be needed to assess whether delayed drought-induced tree mortality amplifies the short-term (< 1 yr) response to drought conditions captured by Lidar and field surveys in this study.

Regional gradients of canopy turnover were weakly correlated with topographic variability, but no clear pattern emerged regarding the influence of topographic position on individual canopy turnover locations seen in other Neotropical forests (Uriarte *et al.*, 2016). The latitudinal gradient in canopy turnover may therefore reflect a combination of factors, including local variability in rainfall, as rainfall deficits are a strong predictor of drought-induced tree mortality (Phillips *et al.*, 2010), or other factors that alter the impact of similar rainfall deficits such as soils and species composition (e.g. Feldpausch *et al.*, 2016).

Branch losses and collateral damage from canopy turnover alter the proportional distribution of AGB in tree crowns and stems for damaged and adjacent canopy and understory trees. Mean values of the proportion of biomass in tree crowns in our study were similar to previous reports (Higuchi *et al.*, 1998), yet individuals varied widely in the distribution of AGB in crown vs stem. Efforts to derive individual tree allometry information directly from Lidar data, including tree height and crown dimensions from airborne Lidar (e.g. Hunter *et al.*, 2013; Jucker *et al.*, 2017) and tree volumes from nondestructive ground sampling using terrestrial laser scanning (e.g. Calders *et al.*, 2015), could rapidly expand existing tropical tree databases to improve allometric models, estimates of above-ground carbon stocks, and the representation of tropical forests in ecosystem models.

The estimated increase in CWD production during drought periods in this study points to the need for a more explicit representation of drought-induced tree mortality and sub-lethal turnover in ecosystem models. Currently, few models mechanistically represent processes that cause drought-driven mortality (van der Molen *et al.*, 2011; Allen *et al.*, 2015; Anderegg *et al.*, 2016), or simulate changes in forest structure and composition in response to drier climates (but see Longo, 2014; Levine *et al.*, 2016). To our knowledge, no model represents sub-lethal turnover from branch loss during droughts. Models generally assume that trees follow allometric relationships, with no loss of woody biomass until death. This representation of tropical forest carbon cycling may either underestimate CWD and associated carbon losses from heterotrophic respiration (e.g. Palace *et al.*, 2008) or overestimate tree mortality if models are parameterized with field measurements of CWD but only whole tree mortality contributes to modeled CWD stocks. Additional work to clarify interannual differences in the rates of branch sloughing (Palace *et al.*, 2008) and modes of tree death (Adams *et al.*, 2017), including hydraulic failure (Rowland *et al.*, 2015), carbon starvation (Doughty *et al.*, 2015) and windthrow (e.g. Chambers *et al.*, 2013), will aid the development of mechanistic models of drought impacts on Amazon forests (Powell *et al.*, 2013; Longo, 2014; Xu *et al.*, 2016). Ecosystem models that can represent interannual variability in canopy turnover may reveal important hysteresis in drought recovery (Keppel-Aleks *et al.*, 2014; Schwalm *et al.*, 2017), as pulses of CWD, reductions in leaf area, reorganization of canopy light environments (Morton *et al.*, 2016; da Costa *et al.*, 2018) and changes in rooting profiles from canopy turnover may extend net carbon emissions following drought periods.

Carbon losses from canopy turnover

The combination of field surveys and repeat Lidar data in this study offers new constraints on the magnitude and variability in CWD production from canopy turnover. Small canopy changes, typical of branch fall events, were widespread (Marvin & Asner, 2016). Large, multiple tree fall events accounted for the largest proportion of turnover area and estimated carbon losses, and were easily distinguishable in multi-temporal high-resolution Lidar data. Multiple branch fall or single tree fall events generated similar changes in canopy area and volume in the Lidar data; large differences in the proportions of the AGB in the stem and crown (see Table S2) underscore the difficulty in estimating carbon losses from these intermediate-sized changes. However, all smaller turnover classes combined (single branch, multiple branch and single tree fall) accounted for only *c.* 20% of estimated carbon losses from canopy turnover. These results contradict previous reports of greater carbon loss from branch fall than tree fall in the Colombian and Peruvian Amazon (Marvin & Asner, 2016). In addition to regional variability in forest structure, composition, and disturbance processes, discrepancies in the proportional contribution from branch fall to carbon losses in this study and the western Amazon may partially result from methodological differences. Lower point densities (2–4 pulses m^{-2}) and larger minimum turnover sizes ($\geq 12\ m^2$) in the analysis by Marvin & Asner (2016), in combination with a height-based classification of branch fall events, may have led to an overestimation of branch turnover area.

Small-area estimation has long been recognized as a challenge for studies of forest carbon stocks using a combination of field and Lidar data (e.g. Meyer *et al.*, 2013; Asner & Mascaro, 2014; Mauya *et al.*, 2015). Overall, changes in canopy volume explained *c.* 30% of the variability in CWD estimated in the field. Moving from the scale of individual turnover events to total changes at 0.25 ha resolution partially balanced problems of under- and over-estimation of CWD from individual turnover events (see Fig. 7), similar to findings in previous biomass change studies in tropical forests (Andersen *et al.*, 2014; Réjou-Méchain *et al.*, 2015). However, increasing the spatial scale does not fundamentally alter the underlying problem – different turnover mechanisms do not generate consistent changes in canopy area, canopy volume and CWD. In particular, field surveys in 2016 confirmed that the loss of large canopy trees does not always generate a gap in tall, multi-layered Amazon forests, even using gap definitions developed specifically for Lidar data (e.g. Hunter *et al.*, 2013; Espírito-Santo *et al.*, 2014; Marvin & Asner, 2016). Average height was > 10 m for all classes (see Table 2), such that it would be difficult to reliably separate branch and tree fall events using a height threshold (Marvin & Asner, 2016).

Our results highlight that Lidar alone may not be sufficient to constrain small changes in canopy and understory forest carbon stocks, as field measurements provide complementary information on the mechanisms and total carbon losses from canopy turnover. In particular, differences in drought sensitivity may alter carbon losses from canopy turnover during drought years, if trees with lower wood density have higher mortality rates in response to soil water deficits (Phillips *et al.*, 2009; Feldpausch *et al.*, 2016). Mortality of smaller trees can also be more easily tracked using inventory plots than airborne Lidar data. It is possible that more frequent Lidar surveys could improve the characterization of biomass loss from canopy turnover based on changes in forest structure immediately following turnover events, rather than the integrated signals of loss and regrowth over the 1–2 yr sampling intervals in this study. Novel methods for routine monitoring of canopy dynamics, including autonomous terrestrial laser scanners (Eitel *et al.*, 2016) or frequent flights with unmanned aerial system platforms, may improve the spatial and temporal sampling of canopy dynamics needed to directly estimate carbon losses from remotely sensed estimates of forest structure. More frequent measurements would also aid efforts to attribute pulses of canopy turnover to specific seasons or phenomena, including potential interaction between drought and wind events.

Conclusions

Airborne Lidar offers an efficient means to characterize Amazon forest dynamics over large areas. Evidence for large interannual variability in canopy turnover in Amazon forests, with ≥ 10 turnover events ha^{-1} yr^{-1} during the 2015–2016 El Niño drought period, suggests that severe drought events alter both short- and long-term regional carbon cycling via changes in canopy structure and associated fluxes of CWD. By linking time series of high-density airborne Lidar data with field measurements of CWD, we clarified the mechanisms that contribute to observed canopy turnover in drought years. Results from this study reaffirm the importance of sub-lethal changes in canopy structure in Amazon forests (Marvin & Asner, 2016), yet our findings contradict the previous work by Marvin & Asner (2016) that branch losses contribute a greater proportion of carbon losses from canopy turnover than tree falls. Using high-resolution repeat Lidar, we found that multiple tree fall events accounted for the largest area of canopy change and > 80% of estimated carbon losses in both sampling intervals. Annualized estimates of carbon losses from canopy turnover in both periods (0.76–1.22 Mg C ha^{-1} yr^{-1}) were comparable to long-term estimates of the net carbon sink in Amazon forests (Brienen *et al.*, 2015), suggesting that interannual variability in canopy turnover contributes to changes in the net carbon balance of Amazon forests during drought years (e.g. Gatti *et al.*, 2014). Finally, our findings also highlight the need to account for both drought-induced mortality and branch losses in ecosystem models to capture time delays in net carbon balance and forest productivity following drought periods.

Author contributions

V.L. and D.C.M. planned and designed the research. V.L. conducted fieldwork. M.K. coordinated Lidar data collection. V.L., D.C.M., M.N.d.S., M.L. and M.S. analyzed and interpreted Lidar results. All authors contributed to the preparation of the manuscript.

ORCID

Douglas C. Morton http://orcid.org/0000-0003-2226-1124
Marcos Longo http://orcid.org/0000-0001-5062-6245

References

Adams HD, Zeppel MJB, Anderegg WRL, Hartmann H, Landhäusser SM, Tissue DT, Huxman TE, Hudson PJ, Franz TE, Allen CD *et al.* 2017. A multi-species synthesis of physiological mechanisms in drought-induced tree mortality. *Nature Ecology & Evolution* 1: 1285–1291.

Aguiar APD, Ometto JP, Nobre C, Lapola DM, Almeida C, Vieira IC, Soares JV, Alvala R, Saatchi S, Valeriano D *et al.* 2012. Modeling the spatial and temporal heterogeneity of deforestation-driven carbon emissions: the INPE-EM framework applied to the Brazilian Amazon. *Global Change Biology* 18: 3346–3366.

Allen CD, Breshears DD, McDowell NG. 2015. On underestimation of global vulnerability to tree mortality and forest die-off from hotter drought in the Anthropocene. *Ecosphere* **6**: 1–55.

Anderegg WRL, Martinez-Vilalta J, Cailleret M, Camarero JJ, Ewers BE, Galbraith D, Gessler A, Grote R, Huang C-y, Levick SR *et al.* 2016. When a tree dies in the forest: scaling climate-driven tree mortality to ecosystem water and carbon fluxes. *Ecosystems* **19**: 1133–1147.

Andersen H-E, Reutebuch SE, McGaughey RJ, d'Oliveira MVN, Keller M. 2014. Monitoring selective logging in western Amazonia with repeat Lidar flights. *Remote Sensing of Environment* **151**: 157–165.

Aragão LEOC, Malhi Y, Roman-Cuesta RM, Saatchi SS, Anderson LO, Shimabukuro YE. 2007. Spatial patterns and fire response of recent Amazonian droughts. *Geophysical Research Letters* **34**: L07701.

Asner GP, Kellner JR, Kennedy-Bowdoin T, Knapp DE, Anderson C, Martin RE. 2013. Forest canopy gap distributions in the southern Peruvian Amazon. *PLoS ONE* **8**: e60875.

Asner GP, Mascaro J. 2014. Mapping tropical forest carbon: calibrating plot estimates to a simple Lidar metric. *Remote Sensing of Environment* **140**: 614–624.

Avitabile V, Herold M, Heuvelink GBM, Lewis SL, Phillips OL, Asner GP, Armston J, Ashton PS, Banin L, Bayol N *et al.* 2016. An integrated pan-tropical biomass map using multiple reference datasets. *Global Change Biology* **22**: 1406–1420.

Brando PM, Balch JK, Nepstad DC, Morton DC, Putz FE, Coe MT, Silvério D, Macedo MN, Davidson EA, Nóbrega CC *et al.* 2014. Abrupt increases in Amazonian tree mortality due to drought–fire interactions. *Proceedings of the National Academy of Sciences, USA* **111**: 6347–6352.

Brando PM, Nepstad DC, Davidson EA, Trumbore SE, Ray D, Camargo P. 2007. Drought effects on litterfall, wood productiod and belowground carbon cycling in an Amazon forest: results of a throughfall reduction experiment. *Philosophical Transactions of the Royal Society of London B* **363**: 1839–1848.

Brienen RJW, Phillips OL, Feldpausch TR, Gloor E, Baker TR, Lloyd J, Lopez-Gonzalez G, Monteagudo-Mendoza A, Malhi Y, Lewis SL *et al.* 2015. Long-term decline of the Amazon carbon sink. *Nature* **519**: 344–348.

Brinck K, Fischer R, Groeneveld J, Lehmann S, Dantas De Paula M, Pütz S, Sexton JO, Song D, Huth A. 2017. High resolution analysis of tropical forest fragmentation and its impact on the global carbon cycle. *Nature Communications* **8**: 14855.

Calders K, Newnham G, Burt A, Murphy S, Raumonen P, Herold M, Culvenor D, Avitabile V, Disney M, Armston J *et al.* 2015. Nondestructive estimates of above-ground biomass using terrestrial laser scanning. *Methods in Ecology and Evolution* **6**: 198–208.

Chambers JQ, Negron-Juarez RI, Marra DM, Di Vittorio A, Tews J, Roberts D, Ribeiro GHPM, Trumbore SE, Higuchi N. 2013. The steady-state mosaic of disturbance and succession across an old-growth Central Amazon forest landscape. *Proceedings of the National Academy of Sciences, USA* **110**: 3949–3954.

Chave J, Andalo C, Brown S, Cairns M, Chambers JQ, Eamus D, Folster H, Fromard F, Higuchi N, Kira T *et al.* 2005. Tree allometry and improved estimation of carbon stocks and balance in tropical forests. *Oecologia* **145**: 87–99.

Chave J, Condit R, Aguilar S, Hernandez A, Lao S, Perez R. 2004. Error propagation and scaling for tropical forest biomass estimates. *Philosophical Transactions of the Royal Society of London B* **359**: 409.

Cook B, Corp L, Nelson R, Middleton E, Morton D, McCorkel J, Masek J, Ranson K, Ly V, Montesano P. 2013. NASA Goddard's Lidar, Hyperspectral and Thermal (G-LiHT) airborne imager. *Remote Sensing* **5**: 4045–4066.

da Costa ACL, Galbraith D, Almeida S, Portela BTT, da Costa M, de Athaydes Silva Junior J, Braga AP, de Gonçalves PHL, de Oliveira AAR, Fisher R *et al.* 2010. Effect of 7 yr of experimental drought on vegetation dynamics and biomass storage of an eastern Amazonian rainforest. *New Phytologist* **187**: 579–591.

da Costa ACL, Rowland L, Oliveira RS, Oliveira AAR, Binks OJ, Salmon Y, Vasconcelos SS, Junior JAS, Ferreira LV, Poyatos R *et al.* 2018. Stand dynamics modulate water cycling and mortality risk in droughted tropical forest. *Global Change Biology* **24**: 249–258.

Doughty CE, Metcalfe DB, Girardin CAJ, Amezquita FF, Cabrera DG, Huasco WH, Silva-Espejo JE, Araujo-Murakami A, da Costa MC, Rocha W *et al.* 2015. Drought impact on forest carbon dynamics and fluxes in Amazonia. *Nature* **519**: 78–82.

Eitel JUH, Höfle B, Vierling LA, Abellán A, Asner GP, Deems JS, Glennie CL, Joerg PC, LeWinter AL, Magney TS *et al.* 2016. Beyond 3-D: the new spectrum of Lidar applications for earth and ecological sciences. *Remote Sensing of Environment* **186**: 372–392.

Espírito-Santo FDB, Gloor M, Keller M, Malhi Y, Saatchi S, Nelson B, Junior RCO, Pereira C, Lloyd J, Frolking S *et al.* 2014. Size and frequency of natural forest disturbances and the Amazon forest carbon balance. *Nature Communications* **5**: 3434.

Fauset S, Johnson MO, Gloor M, Baker TR, Monteagudo MA, Brienen RJW, Feldpausch TR, Lopez-Gonzalez G, Malhi Y, ter Steege H *et al.* 2015. Hyperdominance in Amazonian forest carbon cycling. *Nature Communications* **6**: 6857.

Feldpausch TR, Lloyd J, Lewis SL, Brienen RJW, Gloor M, Monteagudo Mendoza A, Lopez-Gonzalez G, Banin L, Abu Salim K, Affum-Baffoe K *et al.* 2012. Tree height integrated into pantropical forest biomass estimates. *Biogeosciences* **9**: 3381–3403.

Feldpausch TR, Phillips OL, Brienen RJW, Gloor E, Lloyd J, Lopez-Gonzalez G, Monteagudo-Mendoza A, Malhi Y, Alarcón A, Álvarez Dávila E *et al.* 2016. Amazon forest response to repeated droughts. *Global Biogeochemical Cycles* **30**: 964–982.

Gatti LV, Gloor M, Miller JB, Doughty CE, Malhi Y, Domingues LG, Basso LS, Martinewski A, Correia CSC, Borges VF *et al.* 2014. Drought sensitivity of Amazonian carbon balance revealed by atmospheric measurements. *Nature* **506**: 76–80.

Hansen MC, Potapov PV, Moore R, Hancher M, Turubanova SA, Tyukavina A, Thau D, Stehman SV, Goetz SJ, Loveland TR *et al.* 2013. High-resolution global maps of 21st-century forest cover change. *Science* **342**: 850.

Higuchi N, dos Santos J, Ribeiro R, Minette L, Biot Y. 1998. Biomass da parte aérea da vegetação da floresta tropical úmida de terra-firme da Amazônia Brasileira. *Acta Amazonica* **28**: 153–166.

Hunter MO, Keller M, Morton D, Cook B, Lefsky M, Ducey M, Saleska S, de Oliveira RC Jr, Schietti J. 2015. Structural dynamics of tropical moist forest gaps. *PLoS ONE* **10**: e0132144.

Hunter MO, Keller M, Victoria D, Morton DC. 2013. Tree height and tropical forest biomass estimation. *Biogeosciences* **10**: 8385–8399.

Jucker T, Caspersen J, Chave J, Antin C, Barbier N, Bongers F, Dalponte M, van Ewijk KY, Forrester DI, Haeni M *et al.* 2017. Allometric equations for integrating remote sensing imagery into forest monitoring programmes. *Global Change Biology* **23**: 177–190.

Keller M, Palace M, Asner GP, Pereira R, Silva JNM. 2004. Coarse woody debris in undisturbed and logged forests in the eastern Brazilian Amazon. *Global Change Biology* **10**: 784–795.

Kellner JR, Clark DB, Hubbell SP. 2009. Pervasive canopy dynamics produce short-term stability in a tropical rain forest landscape. *Ecology Letters* **12**: 155–164.

Keppel-Aleks G, Wolf AS, Mu M, Doney SC, Morton DC, Kasibhatla PS, Miller JB, Dlugokencky EJ, Randerson JT. 2014. Separating the influence of temperature, drought, and fire on interannual variability in atmospheric CO_2. *Global Biogeochemical Cycles* **28**: 1295–1310.

Le Quéré C, Andrew RM, Canadell JG, Sitch S, Korsbakken JI, Peters GP, Manning AC, Boden TA, Tans PP, Houghton RA *et al.* 2016. Global carbon budget 2016. *Earth System Science Data* **8**: 605–649.

Levine NM, Zhang K, Longo M, Baccini A, Phillips OL, Lewis SL, Alvarez-Dávila E, Segalin de Andrade AC, Brienen RJW, Erwin TL *et al.* 2016. Ecosystem heterogeneity determines the ecological resilience of the Amazon to climate change. *Proceedings of the National Academy of Sciences, USA* **113**: 793–797.

Lewis SL, Brando PM, Phillips OL, van der Heijden GMF, Nepstad D. 2011. The 2010 Amazon drought. *Science* **331**: 554.

Lloyd J, Gloor EU, Lewis SL. 2009. Are the dynamics of tropical forests dominated by large and rare disturbance events? *Ecology Letters* **12**: E19–E21.

Longo M. 2014. Amazon forest response to changes in rainfall regime: results from an individual-based dynamic vegetation model. PhD thesis, Harvard University, Cambridge, MA, USA.

Longo M, Keller M, dos-Santos MN, Leitold V, Pinagé ER, Baccini A, Saatchi S, Nogueira EM, Batistella M, Morton DC. 2016. Aboveground biomass variability across intact and degraded forests in the Brazilian Amazon. *Global Biogeochemical Cycles* 30: 1639–1660.

Marvin DC, Asner GP. 2016. Branchfall dominates annual carbon flux across lowland Amazonian forests. *Environmental Research Letters* 11: 094027.

Mauya EW, Hansen EH, Gobakken T, Bollandsås OM, Malimbwi RE, Næsset E. 2015. Effects of field plot size on prediction accuracy of aboveground biomass in airborne laser scanning-assisted inventories in tropical rain forests of Tanzania. *Carbon Balance and Management* 10: 10.

Meyer V, Saatchi SS, Chave J, Dalling JW, Bohlman S, Fricker GA, Robinson C, Neumann M, Hubbell S. 2013. Detecting tropical forest biomass dynamics from repeated airborne Lidar measurements. *Biogeosciences* 10: 5421–5438.

van der Molen MK, Dolman AJ, Ciais P, Eglin T, Gobron N, Law BE, Meir P, Peters W, Phillips OL, Reichstein M et al. 2011. Drought and ecosystem carbon cycling. *Agricultural and Forest Meteorology* 151: 765–773.

Morton DC, Rubio J, Cook BD, Gastellu-Etchegorry JP, Longo M, Choi H, Hunter M, Keller M. 2016. Amazon forest structure generates diurnal and seasonal variability in light utilization. *Biogeosciences* 13: 2195–2206.

Nepstad DC, Tohver IM, Ray D, Moutinho P, Cardinot G. 2007. Mortality of large trees and lianas following experimental drought in an Amazon forest. *Ecology* 88: 2259–2269.

Palace M, Keller M, Silva H. 2008. Necromass production: studies in undisturbed and logged Amazon forests. *Ecological Applications* 18: 873–884.

Palace M, Keller M. 2008. Necromass production: studies in undisturbed and logged Amazon forests. *Ecological Applications* 18: 873–884.

Pan Y, Birdsey RA, Fang J, Houghton R, Kauppi PE, Kurz WA, Phillips OL, Shvidenko A, Lewis SL, Canadell JG et al. 2011. A large and persistent carbon sink in the world's forests. *Science* 333: 988–993.

Phillips OL, Aragão LEOC, Lewis SL, Fisher JB, Lloyd J, López-González G, Malhi Y, Monteagudo A, Peacock J, Quesada CA et al. 2009. Drought sensitivity of the Amazon rainforest. *Science* 323: 1344.

Phillips OL, van der Heijden G, Lewis SL, López-González G, Aragão LEOC, Lloyd J, Malhi Y, Monteagudo A, Almeida S, Dávila EA et al. 2010. Drought–mortality relationships for tropical forests. *New Phytologist* 187: 631–646.

Powell TL, Galbraith DR, Christoffersen BO, Harper A, Imbuzeiro HMA, Rowland L, Almeida S, Brando PM, da Costa ACL, Costa MH et al. 2013. Confronting model predictions of carbon fluxes with measurements of Amazon forests subjected to experimental drought. *New Phytologist* 200: 350–365.

Réjou-Méchain M, Tymen B, Blanc L, Fauset S, Feldpausch TR, Monteagudo A, Phillips OL, Richard H, Chave J. 2015. Using repeated small-footprint Lidar acquisitions to infer spatial and temporal variations of a high-biomass Neotropical forest. *Remote Sensing of Environment* 169: 93–101.

Rice AH, Pyle EH, Saleska SR, Hutyra L, Palace M, Keller M, de Camargo PB, Portilho K, Marques DF, Wofsy SC. 2004. Carbon balance and vegetation dynamics in an old-growth Amazonian forest. *Ecological Applications* 14: 55–71.

Rowland L, da Costa ACL, Galbraith DR, Oliveira RS, Binks OJ, Oliveira AAR, Pullen AM, Doughty CE, Metcalfe DB, Vasconcelos SS et al. 2015. Death from drought in tropical forests is triggered by hydraulics not carbon starvation. *Nature* 528: 119.

Schwalm CR, Anderegg WRL, Michalak AM, Fisher JB, Biondi F, Koch G, Litvak M, Ogle K, Shaw JD, Wolf A et al. 2017. Global patterns of drought recovery. *Nature* 548: 202–205.

Simard M, Pinto N, Fisher JB, Baccini A. 2011. Mapping forest canopy height globally with spaceborne Lidar. *Journal of Geophysical Research: Biogeosciences* 116: G04021.

Tropical Rainfall Measuring Mission, TRMM. 2011. TRMM (TMPA/3B43) Rainfall Estimate L3 1 month 0.25 degree x 0.25 degree V7. Goddard Earth Sciences Data and Information Services Center (GES DISC), Greenbelt, MD, USA, [WWW document] URL https://disc.gsfc.nasa.gov/datacollection/TRMM_3B43_7.html [accessed January 2018].

Uriarte M, Schwartz N, Powers JS, Marín-Spiotta E, Liao W, Werden LK. 2016. Impacts of climate variability on tree demography in second growth tropical forests: the importance of regional context for predicting successional trajectories. *Biotropica* 48: 780–797.

van der Werf GR, Randerson JT, Giglio L, van Leeuwen TT, Chen Y, Rogers BM, Mu M, van Marle MJE, Morton DC, Collatz GJ et al. 2017. Global fire emissions estimates during 1997–2016. *Earth System Science Data* 9: 697–720.

Williamson GB, Laurance WF, Oliveira AA, Delamônica P, Gascon C, Lovejoy TE, Pohl L. 2000. Amazonian tree mortality during the 1997 El Niño drought. *Conservation Biology* 14: 1538–1542.

Xu X, Medvigy D, Powers JS, Becknell JM, Guan K. 2016. Diversity in plant hydraulic traits explains seasonal and inter-annual variations of vegetation dynamics in seasonally dry tropical forests. *New Phytologist* 212: 80–95.

Zhang K, Chen S-C, Whitman D, Shyu M-L, Yan J, Zhang C. 2003. A progressive morphological filter for removing nonground measurements from airborne LIDAR data. *IEEE Transactions on Geoscience and Remote Sensing* 41: 872–882.

Supporting Information

Additional Supporting Information may be found online in the Supporting Information tab for this article:

Fig. S1 Estimated total annual precipitation and maximum cumulative water deficit (MCWD; Aragão *et al.*, 2007) from satellite and meteorological station data capture the 2015–2016 El Niño drought.

Fig. S2 The distribution of maximum canopy heights within turnover events was similar between the 2013–2014 and 2014–2016 intervals.

Fig. S3 Relative error between observed tree mass ($n = 18$) and estimated above-ground biomass from six different allometric models (see Table S1).

Table S1 Whole tree measurements from coarse woody debris surveys in 2016 were compared to predicted above-ground biomass (AGB) using six allometric equations for tropical forest trees following methods described by Chave *et al.* (2004, 2005)

Table S2 Whole tree measurements from coarse woody debris surveys in canopy turnover areas and estimated above-ground biomass from allometric models of tropical forest trees (see Table S1)

Please note: Wiley Blackwell are not responsible for the content or functionality of any Supporting Information supplied by the authors. Any queries (other than missing material) should be directed to the *New Phytologist* Central Office.